EAI Endorsed Transactions
on Energy Web
Research Article EAI.EU

A fault diagnosis and location method for power grid simulators based on voltage threshold and MCNN

Jinyue Su[1,a], Yingwen Yang[1], YiLin Yu[1], Yueshuo Li[2,b], Shiwei Zhao[1], Zhidong Wang[1*], Ling Yang[1], Fengqiang Deng[1]

[1] School of Electrical Engineering, South China University of Technology, Guangzhou 510800, China
[2] School of Computer Science and Engineering, South China University of Technology, Guangzhou 510800, China

Abstract

To accommodate the testing requirements of high-power wind turbines, this paper designs a power grid simulator topology and investigates fault diagnosis and localization methods by integrating mathematical models and neural networks. To address the drawback of lengthy computation times associated with intelligent diagnostic methods, this paper employs a threshold-based approach using voltage mathematical models to achieve rapid preliminary diagnostics. To address the positioning challenges brought about by symmetrical structures, a multi-layer convolutional neural network (MCNN) model is utilized to achieve accurate positioning. To tackle the issue of insufficient fault samples, a sliding window technique and frequency domain transformation methods are applied to expand the sample set, enabling the diagnosis and localization of 36 types of faults. This paper builds an inverter-side model of the power grid simulator using Simulink to verify the proposed method. And the diagnostic accuracy rate reaches 100%, and the overall localization accuracy exceeds 96%.

Keywords: Power Grid Simulator, MCNN, Frequency Domain Transformation, Sliding Window Method, Sample Expansion

Received on 12 March 2025, accepted on 19 July 2025, published on 26 September 2025

doi: 10.4108/ew.10406

1. Introduction

The large-scale integration of wind turbine units into the power grid will lead to a decrease in grid inertia [1,2], and may result in significant problems such as voltage deviation, frequency deviation [3,4], and increased harmonic content [5]. In response to the new characteristics of the power grid brought about by wind power grid connection, wind turbine units must undergo grid adaptability tests on the test platform before grid connection [6].

The grid simulator, as the core equipment of the ground test platform for wind power generation [7], has the functions shown in Figure 1. It needs to accurately simulate the new characteristics of the grid and test the performance of the wind turbine. Currently, the existing grid simulators in the industry are mostly two-level or three-level low-power grid simulators, with a lower working frequency and less accurate simulation of grid behavior. To meet the testing requirements of large-scale wind turbine units, the modular multilevel converter (MMC) grid simulator has emerged. Its main feature lies in the ability to simulate high-order harmonics in the grid and achieve independent control of the three phases. However, the MMC grid simulator is composed of multiple cascaded H-bridge inverters connected in series. The number of insulated gate bipolar transistors (IGBTs) inside it is significantly more than that of traditional low-level grid simulators, which increases the failure probability of the grid simulator. Once an IGBT fails, it may lead to incorrect judgment of the performance of the wind turbine. In addition, because the diagonal tubes of the H-bridge inverter are turned on alternately, the transistors at the diagonal position of the same module have symmetry. Due to the three-phase independent control of the power grid simulator, transistors at the same position in different modules also have symmetry.

* Corresponding author: Email: zdwang@scut.edu.cn, [a]1911292732@qq.com; [b]2928361457@qq.com

The fault characteristics of symmetrical transistors are similar, which poses difficulties for fault location and repair. Therefore, in order to improve the reliability and availability of grid simulators and provide strong basis for formulating fault-tolerant strategies, it is necessary to study fast fault diagnosis and precise positioning methods applicable to MMC grid simulators[8].

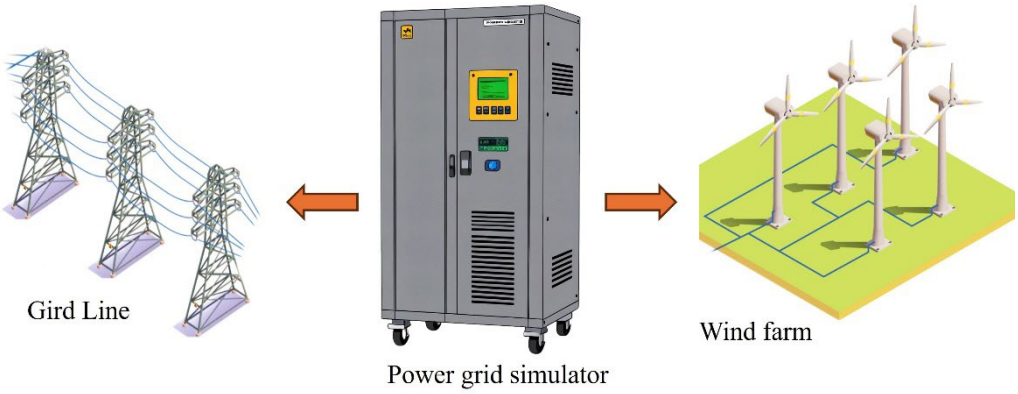

Figure 1. The functions of the power grid simulator

The fault characteristics of symmetrical tubes are extremely subtle and are difficult to distinguish with the naked eye. The traditional method of setting characteristic thresholds for faults cannot achieve precise fault location at the specific fault tubes, which affects the operation and maintenance efficiency of the power grid simulator.

The fault diagnosis and location method based on neural networks can capture the subtle differences in fault characteristics and has obvious advantages in precise location. However, the fault diagnosis process is time-consuming, which is not conducive to the safe operation of the power grid simulator. At present, most intelligent diagnosis methods based on neural networks are limited by the assumption that there are sufficient samples and the data sets are in the same distribution. However, the existing fault samples of large-scale power grid simulators are not complete, and the cost of manual fault experiments is too high, making sample collection difficult, resulting in poor generalization and robustness of the models.

Furthermore, during the process of using neural networks to diagnose and identify faults in the power grid simulator, it was found that simple CNN models have relatively low recognition accuracy. How to establish a high-precision model using a small number of fault samples and improve the diagnostic speed are urgent problems to be solved in the fault diagnosis of the power grid simulator.

2. Topology design of the power grid simulator

In response to the functional requirements of the high-power fan power grid simulator, this paper explores the methods for rapid fault detection and precise location on the inverter side of the power grid simulator. A seven-level MMC type power grid simulator is designed in this paper, and its inverter side is simulated and modeled using Simulink.

2.1. Topology design and working principle

In order to improve the waveform quality and control flexibility when simulating the grid characteristics by the simulator, this paper designs a modular multilevel structure grid simulator with independent control for each phase [9]. The rectification circuit selects a three-phase PWM rectifier to generate a stable DC voltage. The inverter circuit adopts three independent groups of inverters, each group consisting of three-unit H-bridge cascaded single-phase inverters. Through the series bridge arm modules, it can effectively reduce the harmonic content and improve the voltage level. The three groups of inverters can respectively output AC voltage waveforms with phase differences of 120° to simulate various working states of the grid. The single-phase topological structure of the grid simulator system is shown in Figure 2.

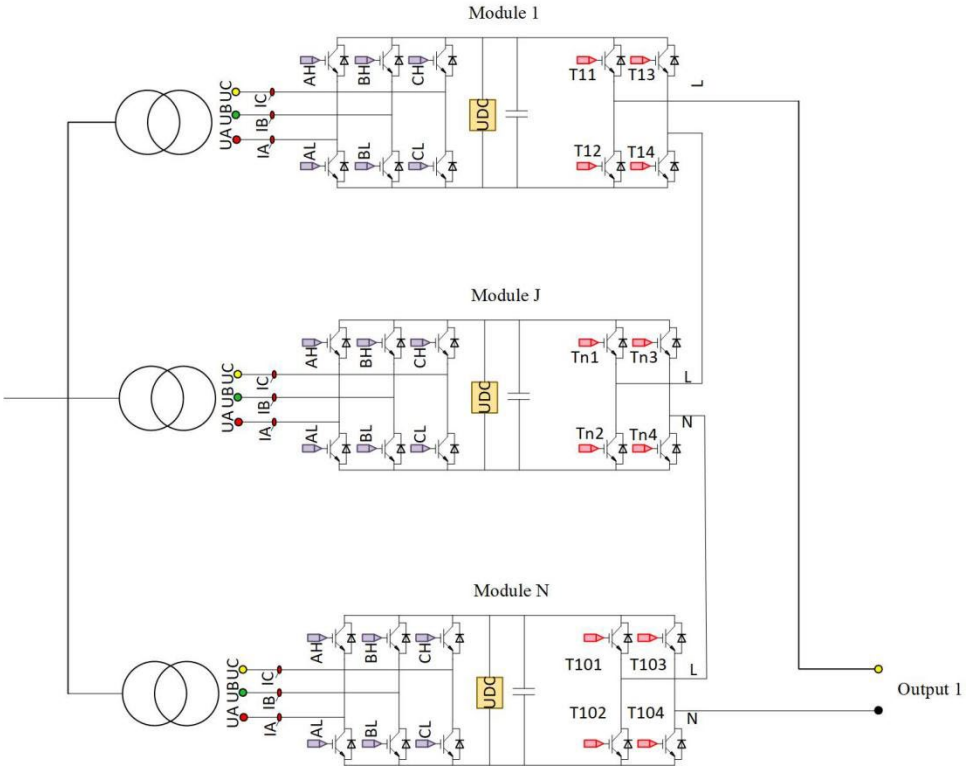

Figure 2. Single-phase topology structure of the power grid simulator

As shown in Figure 2, the H-bridge inverter can convert the DC voltage Udc output by the three-phase PWM rectifier into an AC voltage output. The controller part has three sampling channels, and the given voltage waveform is set through the DSP digital control chip. One H-bridge unit can output three levels: Udc, 0, and -Udc. When three H-bridge inverters are connected in series, they can output 7 voltage levels: 3Udc, 2Udc, Udc, 0, -Udc, -2, Udc, and -3Udc. By writing the control strategy for the inverter switches, the output voltage waveform of the power grid simulator can be set [9].

The MMC type power grid simulator has the advantages of modularization and scalability, but it suffers from the problem of reduced reliability due to the large number of switch quantities. Therefore, it is necessary to develop a fault rapid diagnosis and precise location method suitable for the MMC type power grid simulator.

2.2. Fault types and fault characteristics of the power grid simulator

This paper first analyzes the types and characteristics of faults in the power grid simulator. The majority of the reasons for the faults in the power grid simulator come from IGBTs. IGBT faults usually fall into two types: short circuit and open circuit. Short circuit faults are easy to detect, while open circuit faults have less obvious characteristics and the diagnostic and location methods are more complex. Without appropriate diagnostic methods, the voltage output waveform of the power grid simulator may be distorted [10], which may lead to incorrect judgments of the performance of the wind turbine generator.

Selecting effective fault characteristics is the foundation for achieving fault diagnosis and location. Literature [11] uses the capacitor voltage of sub-modules as the fault characteristic, but this method is not applicable to the power grid simulator. Literature [12] proposes using high-frequency harmonics as the fault characteristic, but when different faults generate similar high-order harmonics, this method can only achieve fault detection but cannot accurately locate the specific position where the fault occurs. There are certain limitations in fault location on the power grid simulator. Literature [10, 12] selects three-phase current as the fault characteristic variable for fault diagnosis and location. Under carrier phase-shift control, the switching timing signal of sub-modules is fixed. When the IGBT in the sub-module has an open circuit fault, the current of this phase cannot flow normally, causing the current waveform to distort. As a result, the current of the other two phases cannot be evenly distributed, resulting in differences in the amplitudes of the three-phase currents. This paper considers 36 types of transistor open circuit fault scenarios, and conducts fault simulation on the built power grid simulator model. Some simulation results are as follows.

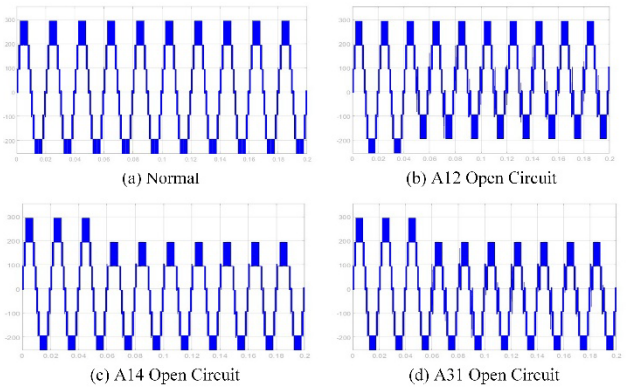

Figure 3. Correlation of phase voltage waveforms for different fault types

As shown in Figure 3, during normal operation, the amplitude of the phase voltage remains stable and there is no DC component within the cycle. When the IGBT of a sub-module fails and becomes open-circuited, the output capability of the sub-module voltage is impaired. The voltage of the sub-module is a component of the phase voltage. The failure of a sub-module will cause the amplitude of the phase voltage to decrease, the waveform to be distorted, and a DC component to appear. Therefore, voltage can be used as a fault diagnosis and preliminary location feature of the fault.

Next, this paper conducts a simulation of the fault current waveform, and presents some of the results as shown in Figure 4.

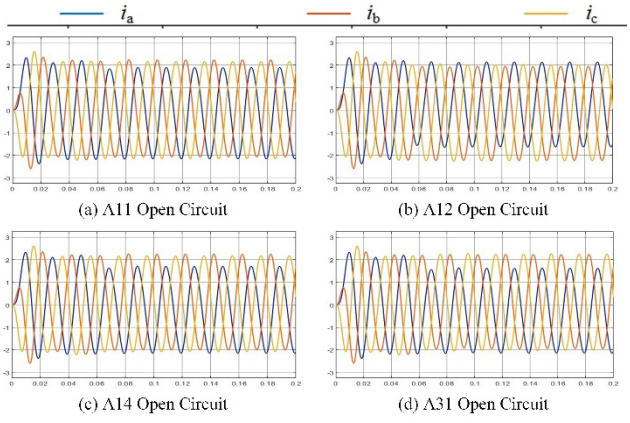

Figure 4. Current waveform arrangement for different fault types

As shown in Figure 4, the current waveforms corresponding to various fault types differ, and the effective fault information can be extracted as the basis for fault location. However, in the same-phase fault types, by comparing the current waveforms of the open circuit of A11 transistor (Figure a) and that of A14 transistor (Figure c), it can be seen that the characteristics of transistor open circuit faults in the same module are similar; by comparing the current waveforms of the open circuit of A11 transistor (Figure a) and that of A31 transistor (Figure d), it can be seen that the waveforms of transistor open circuit faults at the same position in different modules are similar, which cannot be distinguished by the naked eye, and after the fault occurs, there is a process where the current waveforms gradually stabilize into a fault waveform. Therefore, the traditional method of setting characteristic thresholds is difficult to achieve fault type identification, and further refinement processing is required.

In conclusion, phase voltage and line current can be used as features for fault diagnosis and location. In fault diagnosis and the location of the faulty phase, the fault characteristics of phase voltage are more obvious, while in locating to a specific transistor, the three-phase line current is more accurate.

3. Rapid diagnosis and precise location methods

The methods for diagnosing and identifying faults in electrical equipment can be classified as: methods based on mechanism models, methods based on experience, and intelligent identification methods. The fault diagnosis and identification methods based on mechanism models and those based on experience have the advantages of short processing time and timely diagnosis. However, the characteristics of each component of the power grid simulator interact with each other, presenting nonlinear and time-varying characteristics, making it difficult to effectively establish a mathematical mechanism model; the fault diagnosis method based on experience requires manual setting of experience thresholds, and due to the similar characteristic waveforms of some fault types, the determination of the experience thresholds is difficult. The intelligent fault identification method can capture the subtle differences in current characteristics and has obvious advantages in precise positioning, but it takes a long time and requires a large number of fault samples as support.

Taking into account the rapidity and accuracy of fault diagnosis and location, as well as the characteristics of fault features, this paper adopts a rapid diagnosis method based on the threshold setting of the phase voltage mechanism model, and a precise location method based on Multiscale Convolutional Neural Network (MCNN) and using line current as the characteristic.

3.1. A rapid fault diagnosis and preliminary location method based on voltage threshold

Principle analysis

This paper analyzes the influence of faults in each switching tube of the cascaded H-bridge inverter on the output voltage. The topology of a single H-bridge unit is shown in Figure 5,

where VD1 and VT4, VD2 and VD3 are two sets of symmetric IGBTs. It is stipulated that the current flows from the DC side to the AC side as the positive direction.

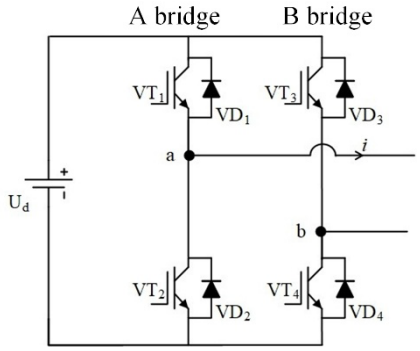

Figure 5. The topological structure of a single H-bridge unit

During normal operation, each single H-bridge unit has four working states. In state 1, the switching tubes VT1 and VT2 are conducting, and the output voltage is 0V. In state 2, the switching tubes VT1 and VT4 are conducting, and the output voltage is +Ud. In state 3, the switching tubes VT2 and VT3 are conducting, and the port output voltage is -Ud. In state 4, the switching tubes VT2 and VT4 are conducting, and the output voltage is 0V. Therefore, VD1 and VD4, VD2 and VD3 are respectively two pairs of symmetrical transistors, which makes the fault characteristics when these two transistors are open-circuited very similar.

In order to analyze the influence of the open-circuit fault of IGBT on the port voltage of the H-bridge unit, each switch tube was set to be open-circuited for analysis. Since VT1 is involved in conduction in states 1 and 2, the fault of VT1 only affects these two states. When VT1 is open-circuited, the current flowing through this switch tube can only be conducted through its reverse-connected diode VD1 for continuation. Due to the unidirectional conductivity of the diode, at this time, only reverse current can pass through. While when the current flows in the forward direction, for state 1, the current originally flowing through VT1 passes through VD2 for continuation, and the port voltage changes from 0V to -Ud. At this time, the working state of the circuit is shown in Figure 6(a); for state 2, the current originally flowing through VT1 also passes through VD2 for continuation, and the port voltage changes from +Ud to 0V. At this time, the working state of the circuit is shown in Figure 6(b).

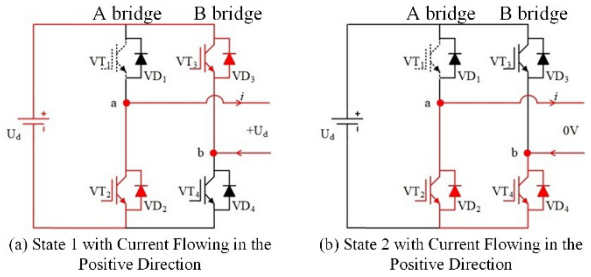

(a) State 1 with Current Flowing in the Positive Direction

(b) State 2 with Current Flowing in the Positive Direction

Figure 6. The operating status of the circuit when VT1 fails

When the VT2 has an open circuit fault, it affects states 3 and 4. Due to the open circuit of VT2, the current originally flowing through VT2 can only continue through VD2. Therefore, the forward current is not affected. When the current reverses, for state 3, the current originally flowing through VT2 is switched to VD1. At this time, the port voltage changes from -Ud to 0V, and the working state of the circuit is shown in Figure 7(a); for state 4, the current of VT2 is switched to VD1, and at this time, the port output voltage changes from 0V to +Ud, and the working state of the circuit is shown in Figure 7(b).

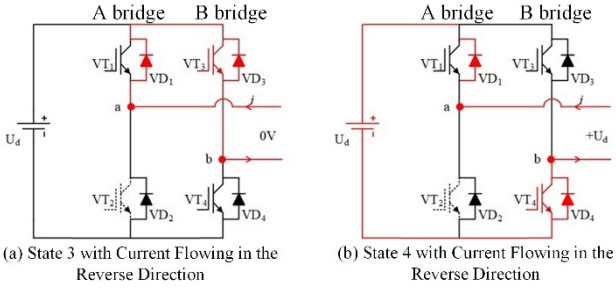

(a) State 3 with Current Flowing in the Reverse Direction

(b) State 4 with Current Flowing in the Reverse Direction

Figure 7. The operating status of the circuit when VT2 fails

The open-circuit fault of VT3 affects states 1 and 3. At this time, the current of VT3 can only flow through VD3 for reverse conduction. Therefore, the open-circuit fault of VT3 affects the reverse flow of the current. When the current flows in the reverse direction, the current that originally flowed through VT3 flows through VD4 for reverse conduction. The port voltage of state 1 changes from 0V to +Ud, and the port voltage of state 3 changes from -Ud to 0V. At this point, the working state of the circuit is as shown in Figure 8.

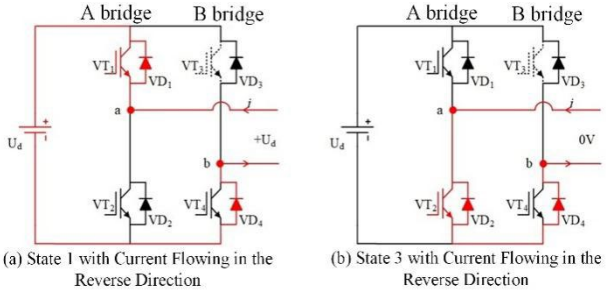

Figure 8. The operating status of the circuit when VT3 fails

As shown in Figure 9, the open-circuit fault of VT4 affects states 2 and 4. Due to the open-circuit fault, when the current flows in the reverse direction, the current of VT4 passes through VD4 for reflow, which does not affect the output voltage at the port; while when the current flows in the forward direction, the current of VT4 flows through VD3 for reflow. At this time, the output voltage of state 2 changes from +Ud to 0V, and the output voltage of state 4 changes from 0V to -Ud.

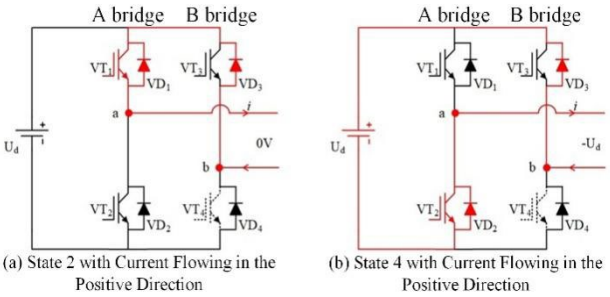

Figure 9. The operating status of the circuit when VT4 fails

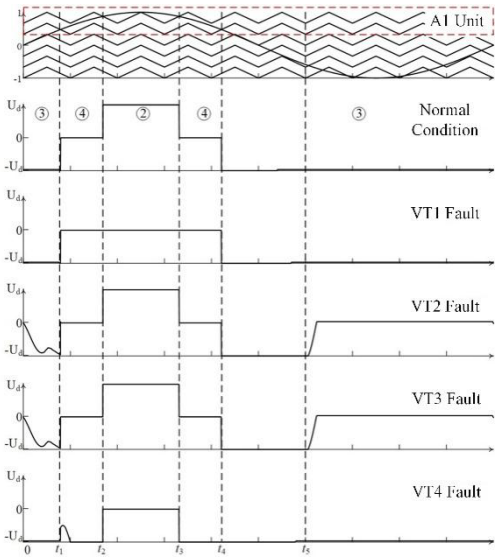

Figure 10. The impact of different switch tube failures on the output voltage of the converter unit

This paper adopts the carrier stacking modulation method. The modulation wave and carrier of each switch tube are shown in Figure 10. From top to bottom, the first and second columns of carriers are the carrier of the a bridge arm and the b bridge arm of the A1 unit. According to the waveform changes of the modulation wave and the carrier, the A1 unit works in five states of 3-4-2-4-3 within one cycle and outputs a three-level voltage. When $0 < t < t_1$, the A1 unit works in state 3. At this time, VT2 and VT3 are conducting, while VT1 and VT4 are turned off. Therefore, only when VT2 and VT3 fail will it affect the output voltage. Since the load is a resistive-inductive load, the voltage leads the current, and the current changes from reverse to positive. When VT2 fails, the output voltage changes from -Ud to 0. When VT3 fails, the output voltage changes from -Ud to 0. When $t_1 < t < t_2$, the A1 unit works in state 4. At this time, VT2 and VT4 are conducting, while VT1 and VT3 are turned off. Only when VT2 and VT4 fail will it affect the output voltage. Since the current is positive at this time, only the failure of VT4 will have an impact. At this time, the output voltage changes from 0 to -Ud. When $t_2 < t < t_3$, the A1 unit works in state 2. At this time, VT1 and VT4 are conducting, while VT2 and VT3 are turned off. Therefore, only when VT1 and VT4 fail will it affect the output voltage. Since the current is positive at this time, the failures of VT1 and VT4 will both cause the output voltage to change from +Ud to 0V. When $t_3 < t < t_4$, the A1 unit works in state 4, which is the same as the working state when $t_1 < t < t_2$. When $t > t_4$ the A1 unit works in state 3, and when $t_4 < t < t_5$, the direction of the current is positive. The failures of VT2 and VT3 will not affect the output current. However, when $t > t_5$, the direction of the current changes from positive to negative, and the failures of VT2 and VT3 will both cause the output voltage to change from -Ud to 0. The working process of A2 unit and A3 unit is similar, so this will not be elaborated further.

Threshold-based diagnostic method using voltage mathematical model

Since this study adopts a three-H-bridge cascaded topology, the output voltage uo of phase A can be expressed as:

$$u_A = u_{A1} + u_{A2} + u_{A3}. \quad (1)$$

In the equation, u_{A1} denotes the terminal voltage of unit A1, u_{A2} represents the output voltage at port A2, and u_{A3} indicates the output voltage of port A3.

When the switching devices operate normally, the output voltage contains no DC component, resulting in zero integral over one period. The voltage integral uA1 can be expressed as:

$$u_{AI} = \int_0^t u_A \mathrm{d}t = \int_0^t (u_{A1} + u_{A2} + u_{A3})\mathrm{d}t. \quad (2)$$

Based on the above analysis, when a switching device fails, the port voltage of the H-bridge unit will exhibit missing voltage levels, resulting in distorted output voltage waveforms and the introduction of a DC component. Specifically, if switching device VT1 or VT4 fails, the maximum output voltage decreases from +3Ud to +2Ud, while the minimum voltage remains largely unchanged. Under this condition, the integral of the output voltage over one period can be approximated as:

$$u_{AI} = \int_0^{T_0/2} 2U_d \sin(\frac{2\pi}{T_0}t)dt + \int_{T_0/2}^{T_0} 3U_d \sin(\frac{2\pi}{T_0}t)dt = -\frac{U_d T_0}{\pi}. \quad (3)$$

Similarly, when switching device VT2 or VT3 fails, the minimum output voltage increases from -3Ud to -2Ud, while the maximum voltage remains essentially unchanged. Under this fault condition, the integral of the output voltage over one period can be approximated as:

$$u_{AI} = \int_0^{T_0/2} 3U_d \sin(\frac{2\pi}{T_0}t)dt + \int_{T_0/2}^{T_0} 2U_d \sin(\frac{2\pi}{T_0}t)dt = \frac{U_d T_0}{\pi}. \quad (4)$$

The computational results demonstrate that a failure in switching device VT1 or VT4 introduces a negative DC component in the output voltage, whereas a failure in VT2 or VT3 produces a positive DC component. Therefore, by calculating the integral values of the phase voltages (A, B, and C) and sampling these integrals at each periodic point, rapid fault detection and phase identification can be achieved.

In this paper, based on the calculated values, the voltage threshold is set to U0 = 5000 V. If the integrated voltage value over four cycles for any phase exceeds this threshold, the system diagnoses a phase fault and triggers an alarm, enabling rapid fault detection and phase localization. Figure 11 illustrates the flowchart of this voltage-threshold-based rapid fault diagnosis and preliminary localization method.

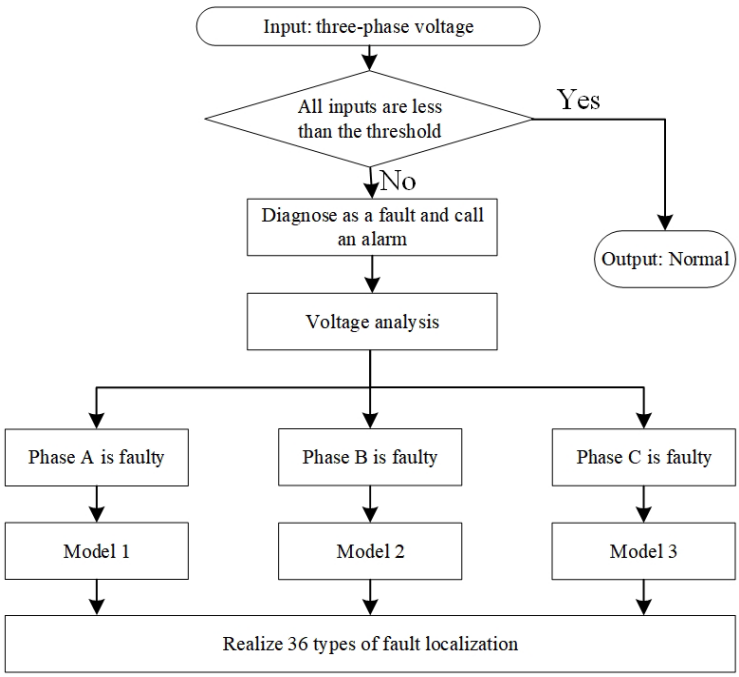

Figure 11. A rapid diagnostic and preliminary positioning method based on voltage threshold

As shown in Figure 11, the proposed method requires training three neural network models to localize faulty power tubes for each phase individually. After identifying the faulty phase via voltage threshold detection, the corresponding model is deployed for precise fault localization.

3.2. MCNN-Based Fault Localization Approach

The threshold-setting method based on the voltage mechanism model can initially locate the faulty phase but cannot pinpoint the specific faulty power tube. Therefore, this paper further investigates an intelligent fault localization approach using three-phase current as the characteristic feature.

Problems in Existing Methods and Prior Research

The neural network-based intelligent localization method excels at capturing subtle correlations and distinctions among fault characteristics, demonstrating significant advantages for fault localization in complex systems.

Pioneering achievements have been made in intelligent diagnostic methods for MMCs [13], providing valuable insights for fault diagnosis and localization in MMC-based grid simulators. Reference [14] employs a 1D Convolutional Neural Network (CNN) to process raw voltage and current data from MMCs for fault localization, while Reference [11]

proposes a Sliding Time Window (STW)-based Feature Extraction Algorithm (FEA) coupled with a 2D CNN for enhanced diagnosis and localization.

However, the aforementioned methods exhibit three critical limitations:

- Directly inputting large volumes of raw voltage and current data as samples may trigger the "curse of dimensionality", leading to prolonged computational delays in intelligent diagnostic methods and potentially compromising the safe operation of grid simulators;
- The aforementioned methods are limited by the assumptions of sufficient sample size and uniform data distribution, while the scarcity of fault data in grid simulators leads to insufficient adaptability of conventional intelligent diagnostic approaches;
- The one-dimensional convolutional neural network (1D CNN) processes univariate data and extracts local features effectively, but exhibits limitations in capturing global contextual relationships across multiple dimensions and handling multi-scale features. While Reference [12] demonstrated successful fault diagnosis for single-phase MMC systems using 1D CNN, the polyphase grid simulator studied in this work generates multidimensional fault characteristics. Consequently, both 1D CNN and 2D CNN show unsatisfactory accuracy in fault diagnosis and identification for this application.

Therefore, it is imperative to develop an intelligent localization method with fault sample augmentation capabilities.

The Multi-scale Convolutional Neural Network (MCNN) employs convolutional kernels of varying scales to enhance fault identification. Smaller kernels capture fine-grained details of fault characteristics, while larger kernels extract global fault information. By integrating these multi-scale features, the model achieves a more comprehensive representation of fault types, significantly improving diagnostic accuracy.

The fusion of multi-scale feature maps enables effective consolidation of hierarchical characteristics. This architecture fully leverages features at different levels, particularly enhancing the model's sensitivity to subtle signatures—making it exceptionally suitable for fine-grained fault identification tasks. Its robust multi-scale processing capability improves recognition robustness for varying fault signatures.

This study proposes the adoption of an MCNN-based approach for fault localization.

Data Preprocessing

For the grid simulator shown in Figure 2, complete three-phase current data is acquired through installed sensors. Due to the scarcity of fault samples in grid simulators, directly using single fault events as training data makes model convergence difficult. To augment fault samples, this paper first employs a sliding window feature extraction algorithm to segment existing fault data [13]. The offline data processing procedure using the sliding window is illustrated in the figure 12.

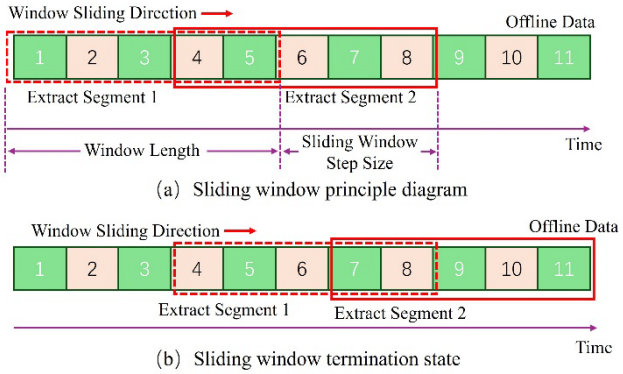

Figure 12. Schematic Diagram of the Sliding Window Feature Extraction Algorithm

Let the total length of the original fault current information be denoted as L_{ori}, with a window of length L_{win} used to segment the original information at a step size L_{step}. After multiple slides, multiple data segments of length L_{win} are obtained. When the window reaches the end of the original data, if the remaining number of samples is less than the step size of the sliding window, the window stops sliding [13]. The number of extracted data segments is then determined as:

$$S = \left\lfloor \frac{L_{ori} - L_{win}}{L_{step}} \right\rfloor + 1 . \quad (5)$$

Through iterative experimentation, this study selects a window length of 8,000 data points (equivalent to 0.08 seconds) and a stride of 4,000 data points (0.04 seconds). The quantity of segmented fault samples is presented in the table 1 below.

Table 1. The number of segmented fault samples

Fault phase	Phase A	Phase B	Phase C
Number of samples	6941	4022	6078

The fault samples from each phase were partitioned into training (76%), testing (20%), and validation (4%) sets. The training and testing sets were used to develop the fault location model, while the validation set evaluated the model's localization accuracy.

Sample Augmentation Using FFT and IFFT

Due to the limited number of available fault samples in the grid simulator, direct model training would result in poor generalization capability. To address this, the present study proposes a frequency-domain transformation approach for sample augmentation. Specifically, fault samples are first converted to the frequency domain via Fourier Transform, where filtering and perturbation operations are applied, before being reconstructed back to the time domain through inverse transformation. As shown in Figure 13, This process generates new fault samples while enhancing both diversity and robustness [15]. The detailed implementation steps are as follows:

Perform Fast Fourier Transform (FFT) on the data samples to convert time-domain signals into frequency-domain signals.

$$X(f)=\int_{n=0}^{N-1}x(n)e^{-j2\pi fn/N}\ . \tag{6}$$

Here, $X(f)$ represents the frequency-domain representation of $x(n)$, where f denotes the frequency variable and N corresponds to the data length.

After introducing noise to the frequency-domain signal, an Inverse Fast Fourier Transform (IFFT) is applied to reconstruct the time-domain signal:

$$x(n)=\frac{1}{N}\sum_{f=0}^{N-1}X(f)e^{j2\pi fn/N}\ . \tag{7}$$

Normalize the augmented fault samples:

$$x'=\frac{x-x_{\min}}{x_{\max}-x_{\min}}\ . \tag{8}$$

Where x and x' represent the original and normalized feature values, respectively, while $x_{\max}$ and $x_{\min}$ denote the maximum and minimum values of the feature set.

The frequency-domain transformation not only expands the fault samples but also smooths their distribution. Notably, its parameter selection is not manually specified, thereby ensuring the diversity of fault samples.

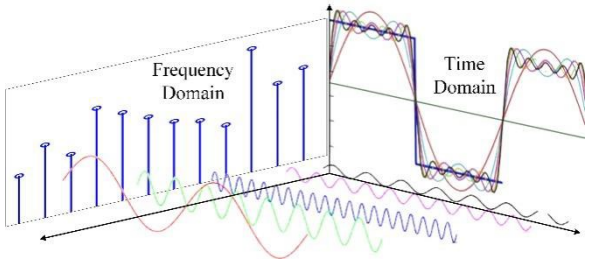

Figure 13. Schematic Diagram of Frequency-Domain Transformation

Multi-scale Convolutional Neural Network (MCNN) Model

Leveraging the extensively augmented fault samples, the MCNN model is employed as both a classification and regression model.

The Multi-scale Convolutional Neural Network (MCNN) model is a multi-scale convolutional neural network that captures features of input data at varying scales through differently sized convolutional kernels or parallel branch structures. Compared to standard CNN architectures, the MCNN achieves superior feature representation and higher accuracy, while improving automation and adaptability. The MCNN model has been successfully applied across diverse domains, including image classification, crowd counting, fault diagnosis, and multimodal fake news detection [16].

Through iterative experimentation, this study selects convolutional kernels with lengths of 3 and 50 (16 kernels each) to extract features from the preprocessed and augmented three-phase current data. The multi-scale features are then concatenated into a single channel to fuse information across different scales. Subsequently, a fully connected layer with 128 nodes further processes and combines the fused features[17,18]. The algorithmic workflow is illustrated in Figure 14.

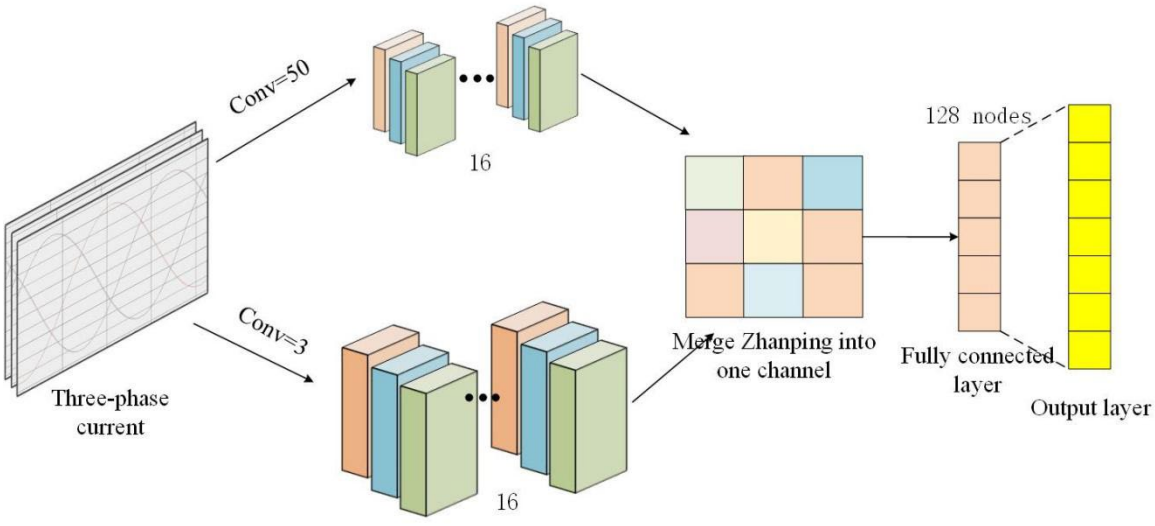

Figure 14. Schematic Diagram of the MCNN (Multi-scale Convolutional Neural Network) Model MCNN

Exploration of Valid Samples

In the dataset, the initial segments represent normal current data, while post-fault current waveforms exhibit a gradual deviation from normal values toward characteristic fault patterns. Using the entire dataset for MCNN training would lead to suboptimal fitting, as segments from different fault types may share similar transitional patterns, thereby "pulling" the model in conflicting directions. To address this, our study trains the MCNN on three distinct time-segmented datasets and evaluates their fault localization performance on a shared validation set. The overall accuracy results are presented in the figure below.

Figure 15. Impact of Time-Segmented Datasets on Overall Training Performance

Statistical analysis was conducted on all accuracy metrics, with the results visualized in the line chart below.

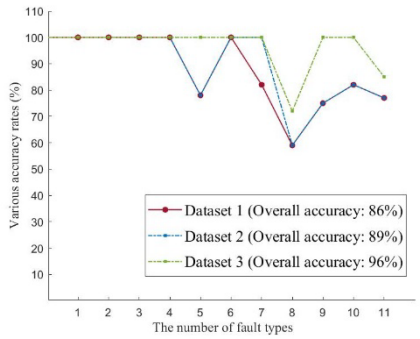

Figure 16. Comparison of Fault-Type Identification Accuracy Across Time-Segmented Datasets

As evident from Figures 15 and 16, the later the training set is in the temporal sequence, the higher its identification accuracy becomes. Since the voltage-threshold-based fault diagnosis method can rapidly detect fault occurrences, fault-type identification prioritizes accuracy. Balancing both timeliness and accuracy, this study selects Dataset 3 to train individual models, resulting in three dedicated models for fault localization across the three phases.

The schematic diagram of the fault localization method using the enhanced MCNN model with augmented fault data is shown in the figure 17.

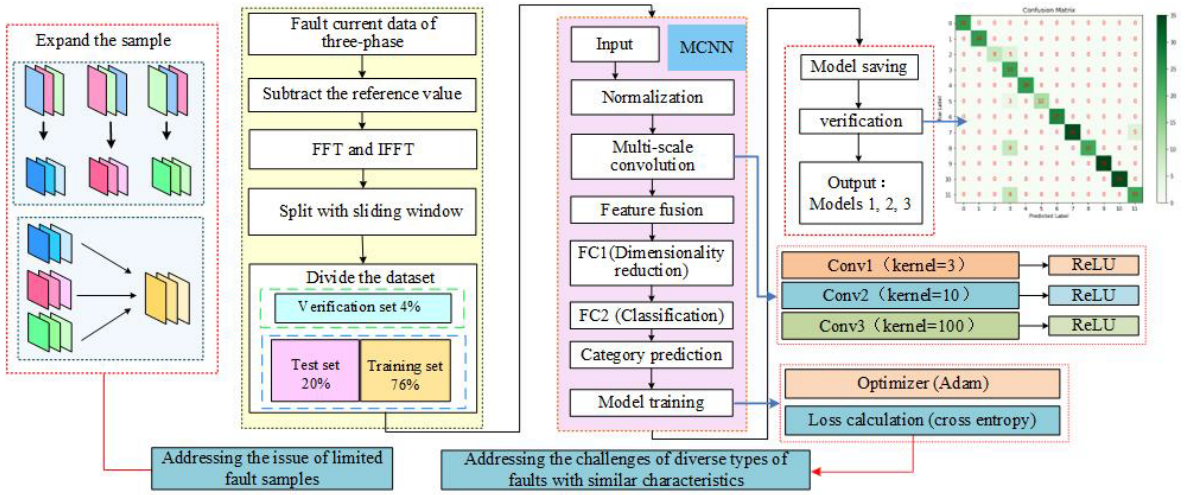

Figure 17. Comparison of Schematic Diagram of the Fault Localization Method Using the Data-Augmented MCNN Model

4. Results

This paper employs Simulink to construct the simulation model of the power grid simulator, with the key circuit parameters detailed in Table 2. By simulating 36 distinct fault scenarios on the inverter side of this simulator, the model acquires both normal operational data and fault data for each phase (A, B, and C) tube. These datasets are utilized to separately train three distinct MCNN positioning models. Finally, this paper uses the validation set to verify the model, and evaluates its classification performance through the confusion matrix and accuracy rate indicators. The relevant results and per-class F1-score breakdowns are shown in Figure 18 and Table 3 respectively.

Table 2. Design parameters of the main circuit

Parameter	Title 2
Rated power	800W
Voltage on the DC side	100V
Switching frequency	10kHz
Sampling frequency	200kHz
Filter inductorL	27mH
Filter capacitorC	

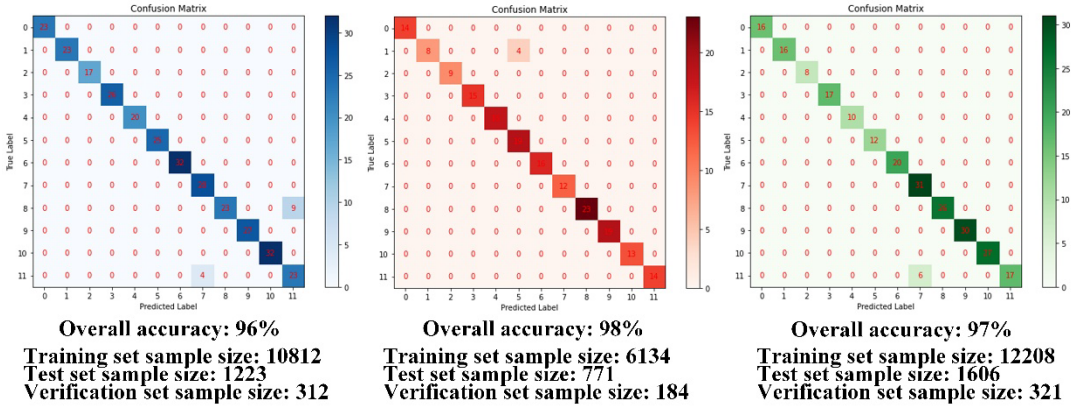

Figure 18. Fault location diagrams for each phase

Table 3. per-class F1-score breakdowns

Fault Types		Precision (%)	Recall (%)	F1-score (%)
A 相	A0~6、A9~10	100	100	100
	A7	87.5	100	93.33
	A8	100	71.88	83.64
	A11	71.88	85.19	77.97
B 相	B0、B2~4、B6~11	100	100	100
	B1	100	66.67	80.00
	B5	82.61	100	90.48
C 相	C0~6、C8~10	100	100	100
	C7	83.78	100	91.17
	C11	100	73.91	85.00

The results show that the fault diagnosis and location method combining voltage threshold with MCNN achieves an accuracy rate of 100% in diagnosis, and the single diagnosis time is at the millisecond level. In fault location, the overall accuracy rate reaches over 96%. Compared with the simple CNN model, the diagnostic accuracy of this method is increased by approximately 4%, the diagnosis time is significantly shortened, and the location accuracy is improved by 1%. Moreover, due to the use of the MCNN model in this method, it has a stronger adaptability to noise and better robustness. Therefore, the efficiency and accuracy of this method in the paper can be seen.

5. Discussion

This paper adopts a fault diagnosis and location method that combines mathematical models with neural networks. It retains the efficiency of the threshold setting method in mathematical models and the ability of intelligent diagnosis to identify subtle features. This enables rapid diagnosis and accurate fault location, which is of great significance in engineering. The rapidity of diagnosis ensures the reliability of operation. During intervals, safety measures and protection measures can be taken. Precise location can reduce the workload for the operation and maintenance and repair of the power grid simulator.

To ensure a high accuracy rate in fault location, the training and testing datasets for the model in this paper are positioned towards the end in the time domain. It means that although this method can provide rapid diagnosis, the location still requires a certain amount of time. This is because the differences in fault currents tend to reach characteristic values slowly, and the distinctions are subtle. At the same time, a fine-tuning model can be established to explore the minimum interval time by testing the effective

dataset, further improving the timeliness of fault location. Additionally, since the probability of simultaneous failure of both tubes and multiple tubes is extremely low, this paper does not conduct related research. The next step of research will consider transfer learning of fault samples under different operating conditions and the identification of simultaneous tube failures and multiple tube failures, further improving the accuracy and generalization. At the same time, the influence of the load on the location results and timeliness can be studied, and test loads can be studied for fault diagnosis and location in engineering applications.

6. Conclusion

This paper integrates mathematical models and intelligent diagnostic methods. By setting fault thresholds through voltage mathematical models, it achieves a 100% accuracy rate in rapid fault diagnosis, addressing the timeliness deficiency of intelligent diagnostic methods. Additionally, Using neural networks to overcome the problem of difficult localization of symmetrical pipe faults. Effective fault datasets are selected through training experiments with adjusted intervals. Fault samples are expanded using the sliding window method and frequency domain transformation, and the MCNN (Multilayer Convolutional Neural Network) model is trained to capture subtle features, achieving a fault localization accuracy of over 96% overall.

Funding

This research was funded by National Key R&D Program of China (Grants No. 2024YFB3411000)

Acknowledgements.

We would like to express our sincere gratitude to the National Key R&D Program of China （Grants No. 2024YFB3411000）for its generous funding of this research. The financial support provided by this program has laid a solid foundation for the smooth progress of the research, enabling us to focus on the research work and devote ourselves to exploring the relevant contents of the research topic.

References

[1] Deng W, Dai N Y, Lao K W, et al. A virtual-impedance droop control for accurate active power control and reactive power sharing using capacitive-coupling inverters[J]. IEEE Transactions on Industry Applications, 2020, 56(6): 6722-6733.

[2] Deng W, Xiao D, Chen M, et al. Multi-regional energy sharing approach for shared energy storage and local renewable energy resources considering efficiency optimization[J]. International Journal of Electrical Power & Energy Systems, 2025, 167: 110592.

[3] Xiong L, Li P, Wu F, et al. Stability enhancement of power systems with high DFlG-windturbine penetration via virtual inertia planning[J. lEEE Transactions on Power Systems, 201934(2): 1352-1361.

[4] Liu J, Xu Y, Dong Z Y, et al. Retirement-driven dynamic VAR planning for voltage stabilityenhancement of power systems with high-level wind power{J]. IEEE Transactions on PowerSystems,2018,33(2):2282-2291.

[5] Shuai Z, Liu D, Shen J, et al. Series and parallel resonance problem of widebandfrequency harmonic and its elimination strategy[J]. lEEE Transactions on Power Electronics. 2014, 29(4):1941-1952.

[6] Li Houxiang, Zhang Yongming, Zhai Hongyu. Research on Topology and Control System of High Power Grid Simulator[J]. Journal of Physics: Conference Series, 2021, 2083(3).

[7] Feke, Chen Guochu. Parameter Design of Grid Simulator Based on Improved Proportional Resonance Controller [J]. Science and Technology Economic Review, 2018, 26(23): 23-24 + 37.

[8] Sobanski Piotr, Miskiewicz Milosz, Bujak Grzegorz, et al. Real Time Simulation of Power Electronics Medium Voltage DC-Grid Simulator[J]. Energies, 2021, 14(21): 7368-7368

[9] Wang Qi. Research on control technology of inverter side of grid simulator based on hierarchical repetitive adaptive control[D]. Nanjing University of Science & Technology, 2023.DOI:10.27241/d.cnki.gnjgu.2023.000561.

[10] Liu Shuxi, Liu Ke, Wang Qianyun, Qu Yufei, Luo Qin. Open-circuit fault diagnosis of MMC sub modules based on modal time-frequency diagrams and the Resnet-BiGRU model[J]. Power System Protection and Control, 2025, 53 (02): 73-88.

[11] Yang Heya, Xing Wenshuo, et al. A Fault Detection and Location Strategy for Sub-module Open-circuit Fault in Modular Multilevel Converters Based on Random Forest Binary Classifier[J].Proceedings of the CSEE, 2023,43(10):3916-3928. DOI:10.13334/j.0258-8013. pcsee. 221115.

[12] PABLO L, RICARDO A, JOSE R. Fault detection on multi-cell converter based on output voltage frequency analysis[J]. IEEE ransactions on Industrial Electronics, 2009, 56(6): 2275-2283.

[13] DENG Fujin, JIN Ming, LIU Chengkai, et al. Switch open-circuit fault localization strategy for MMCs using sliding-time window based features extraction algorithm[J]. IEEE Transactions on Industrial Electronics, 2021

[14] S. Kiranyaz, A. Gastli, L. Ben-Brahim, N. Al-Emadi, and M. Gabbouj, “Real time fault detection and identification for MMC using 1-D con-volutional neural networks,” IEEE Trans. Ind. Electron., vol. 66, no. 11, pp. 8760–8771, Nov. 2019.

[15] J. Liu and Y. Ren, "A General Transfer Framework Based on Industrial Process Fault Diagnosis Under Small Samples," in IEEE Transactions on Industrial Informatics, vol. 17, no. 9, pp. 6073-6083, Sept. 2021, doi: 10.1109/TII.2020.3036159.

[16] M. Arjovsky, S. Chintala, and L. Bottou, “Wasserstein generative adversarial networks,” in Proc. 34th Int. Conf. Mach. Learn., vol. 70, Aug. 2017, pp. 214–223.

[17] Choudhary, Sarika, and Nishtha Kesswani. "Analysis of KDD-Cup’99, NSL-KDD and UNSW-NB15 datasets using deep learning in IoT." Procedia Computer Science 167 (2020): 1561-1573.

[18] Mahalakshmi, G., et al. "Intrusion detection system using convolutional neural network on UNSW NB15 dataset."

Advances in Parallel Computing Technologies and Applications. IOS Press, 2021. 1-8.